Vertex functions for confined quarks in momentum-space quark-hadron models

L. S. Celenza, C. M. Shakin, Wei-Dong Sun, J. Szweda, and Xiquan Zhu
Department of Physics and Center for Nuclear Theory,
Brooklyn College of the City University of New York, Brooklyn, New York 11210
(Received 2 April 1993; revised manuscript received 9 December 1993)

We consider the excitation of a quark-antiquark pair from the vacuum by a scalar-isoscalar source and define a vertex function for that process. We construct an equation for the vertex function, making use of a quark-antiquark interaction that describes confinement, and solve for the vertex function in a projected space defined using positive- and negative-energy projection operators constructed in terms of Dirac spinors. The solution of our projected equation yields a vertex function that is equal to zero when both the quark and the antiquark go on the mass shell. This result allows us to study quark dynamics in momentum space in the presence of a confining interaction. The role of our vertex function in extending the Nambu–Jona-Lasinio model to include a description of confinement is considered. It may be seen that various amplitudes are free of the discontinuities that arise when the quark and antiquark go on the mass shell and, therefore, dispersion relations may be developed that are free of unphysical singularities. (In this work, we are mainly interested in the scalar-isoscalar $q\bar{q}$ channel; however, the analysis may be extended to include sources carrying other quantum numbers.) The projected equations also allow for systematic approximations, such as the neglect of retardation and the neglect of pair-current effects, etc. Solutions are presented for the coupled equations obtained with the use of projection operators. We conclude that the use of projection operators, supplemented by the neglect of retardation, is a useful procedure for the calculation of vertex functions of the type considered in this work.

PACS number(s): 12.38.Aw, 12.39.Pn, 14.65.−q

I. INTRODUCTION

We should say at the outset that we are not here interested in studying the bound states of mesons and baryons in the presence of an interaction that describes confinement. Indeed, there are quite satisfactory methods available for solving such problems. (The solutions are usually made in coordinate space, since the confining potential is most easily represented in coordinate space.) The problem that does concern us is the calculation of hadronic current correlators [1] when we make use of quark models. The theory that we have developed for mesonic correlators [2,3] describes the coupling of quark-antiquark states to states of the two-pion continuum (or the π-ρ continuum in the case of the axial-vector isovector correlator [3]). Thus, we consider a coupled-channel system of $q\bar{q}$ states and states of two (or more) mesons. In such problems it is quite useful to be able to use dispersion relations. However, standard many-body techniques, when applied to this problem, would yield amplitudes with a cut structure starting at $P^2 = 4m_q^2$, corresponding to the quark and antiquark going on the mass shell. (Here, m_q is the constituent quark mass.) That feature would eliminate the possibility of writing meaningful dispersion relations. Therefore, we need a formalism which eliminates the $q\bar{q}$ cuts from the various amplitudes of the model. It is one goal of this work to show how one may formulate a model in which such $q\bar{q}$ cuts are absent in the relevant kinematical domain.

It is also important to note that the vertex function we consider in this work is not a vertex function for the *full* $q\bar{q}$ interaction, but only describes effects of the confining field. The full vertex function can be characterized in terms of the $q\bar{q}$ T matrix, appropriately defined [2]. That T matrix would contain (complex) poles associated with the formation of mesons as $q\bar{q}$ bound states. For example, in Ref. [2], we show how the ρ meson emerges in the study of $q\bar{q}$ dynamics in the vector-isovector $q\bar{q}$ channel.

The vertex function studied in this work does not contain the meson resonance poles, since it is only the vertex for the confining field. If the confining field itself generates bound states, these would appear in our vertex function. However, for the confining fields we consider, such bound states appear at higher energies than those relevant for our problem. (See the Appendix.)

The utility of studying the vertex for the confining field in isolation may be seen in our analysis of hadronic current correlation functions [2]. In Ref. [2] we consider the effects of the short-range $q\bar{q}$ interaction of the Nambu–Jona-Lasinio model [4], the confining interaction and the coupling of the $q\bar{q}$ states to the two-pion continuum. The expressions for the hadronic current correlator are such that the effects of the three interactions mentioned above may be separately identified. The vertex for the confining field appears naturally as an element of that formalism and is the object of our study. (See Sec. IV.)

Note that, in the case of hadronic current correlation functions, the momentum-space correlator depends upon one, or more, scalar functions which are functions of the square of a single four-vector, P^2. In the simplest example, the scalar-isoscalar current correlator is

 ©1995 The American Physical Society

$$-iC_S(P^2) = \int d^4x e^{iP\cdot x}\langle 0|T[\bar{q}(x)q(x)\bar{q}(0)q(0)]|0\rangle, \quad (1.1)$$

where $C_S(P^2)$ is the function of interest and $q(x)$ is the quark field. Thus, we see that there is a continuous variable P^2, in the problem. (If $\mathbf{P}$=0, we can take P^0 to be the relevant variable.) Therefore, the calculation of correlation functions is unlike the calculation of bound-state properties. In the latter case, we have an eigenvalue value problem that requires we determine specific values of $P^2 = M^2$.

A description of confinement in models of hadrons can be made in various ways. In some bag or soliton models, confinement is introduced as a property of the vacuum, where a free quark or gluon is taken to have infinite energy. However, in potential models of meson structure, a linear potential is often used to represent confinement. That potential has its orgin in the formation of a flux tube between a quark and an antiquark as they move apart. In this work we consider confinement as implemented by a linear potential. (See Sec. III.)

There are quark models, based upon the Nambu–Jona-Lasinio (NJL) model [4], that have been extensively studied, but which do not describe confinement. The NJL model provides an elementary model of dynamical breaking of chiral symmetry. In the study of that model, one can use a full array of many-body techniques and may construct quark self-energy operators and associated Green's functions. The model provides values of the vacuum quark condensate, the pion mass, and the pion decay constant in terms of a few parameters. These include a coupling constant G_S, a momentum cutoff Λ, and a current quark mass m_q^0, when we consider the flavor-SU(2) version of the model. In order to motivate the calculations we report here, we will review a few features of the NJL model. The Lagrangian is

$$\mathcal{L}(x) = \bar{q}(x)(i\not{\partial} - m_q^0)q(x) + G_S/2\{[\bar{q}(x)q(x)]^2 + [\bar{q}(x)i\gamma_5\boldsymbol{\tau}q(x)]^2\}. \quad (1.2)$$

Now, consider the scattering amplitude for a scalar-isoscalar $q\bar{q}$ channel. Suppressing reference to matrices in Dirac, color, and isospin space, we can write the scattering matrix as [5]

$$t_S(P^2) = -\frac{G_S}{1 - G_S J_S(P^2)}, \quad (1.3)$$

where $J_S(P^2)$ is the quark-loop integral shown in Fig. 1(a). Note that

$$-iJ_S(P^2) = (-1)n_c n_f \mathrm{Tr}\int \frac{d^4k}{(2\pi)^4} iS(P/2+k) \times iS(-P/2+k), \quad (1.4)$$

where $S(p) = [\not{p} - m_q + i\epsilon]^{-1}$, n_c, is the number of colors, and n_f is the number of flavors. Further, m_q is the constituent mass obtained by solving the gap equation of the NJL model. One readily sees that $J_S(P^2)$ has a cut starting at $P^2 = 4m_q^2$ that corresponds to the quark and antiquark becoming physical particles. This feature clearly limits the application of the NJL model to relatively small values of P^2. However, a number of researchers have disregarded this problem and have made predications concerning the properties of the ρ, ω, and more massive mesons, for example [6]. (Note that $m_\omega^2 > 4m_q^2$, etc.)

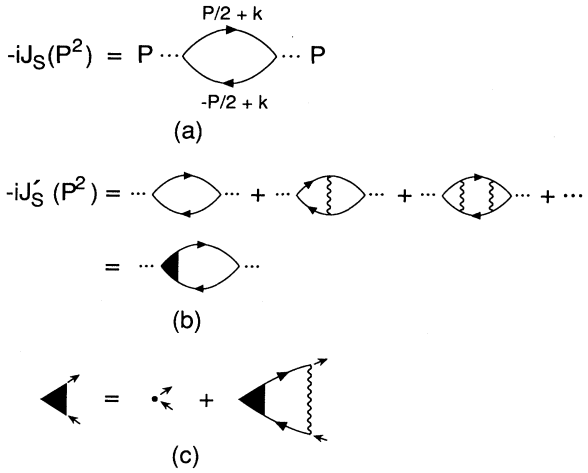

FIG. 1. (a) Quark-loop integral that arises in the analysis of the NJL model. A four-dimensional integral over k is implied. [See Eq. (1.3).] (b) Inclusion of a long-range potential (wavy line) in the calculation of the quark-loop integral. The filled triangular region represents the vertex function of that potential. (c) An integral equation for the vertex function is represented in a schematic fashion. (See Fig. 2.)

It would be useful to extend the NJL model to describe confinement. One way to do this is to add a long-range potential to the model that already has a mechanism that gives rise to chiral symmetry breaking. Such a program has been discussed in fairly general terms by Gross and Milana [7,8]. One particularly useful feature of their analysis is their ability to "decouple" the discussion of confinement from that of chiral-symmetry breaking [8]. We do not wish to repeat their argument here, except to note that their result depends upon a constraint satisfied by the long-range potential in their formalism that is the relativistic analog of a condition in the nonrelativistic theory that would require the linear (confining) potential to vanish at the orgin, that is $V_L(r) = 0$ for $r = 0$. Because of the possibility of considering the confinement problem independently of chiral symmetry breaking [8], in this work we will limit ourselves to the discussion of only the long-range potential. (That potential is denoted by a wavy line in the figures.)

Consider the sum of diagrams in the upperpart of Fig. 1(b). These diagrams serve to define a vertex, the filled triangular shape in Fig. 1(b). In Fig 1(c), we show the equation satisfied by the vertex, where, for the scalar-isoscalar channel, the driving term is unity in the Dirac, flavor, and color space. (Note that the Bethe-Salpeter equation for a *bound state* would be homogeneous. That is, there would be no driving term, and we would have

an eigenvalue problem. That feature characterizes the bound-state problem considered by Gross and Milana.)

The notation we will adopt is shown in Fig 2(a). In general, the scalar-isoscalar vertex function is a Dirac matrix that depends on three variables, $\hat{\Gamma}_{\alpha\beta}(P^2, P\cdot k, k^2)$; however, we will consider various reduction schemes that convert the four-dimensional equation for the vertex to three-dimensional equation for scalar functions of two variables. The number of unknown scalar functions considered depends upon the reduction scheme. If we neglect retardation, we may solve a three-dimensional equation for a function of two variables or, in the general case, coupled three-dimensional equations for two functions of two variables. [Since P^0 appears as a *parameter* in these equations, functions of P^0 and $|\mathbf{k}|$ may be considered to be functions of a single variable. In the following, we will sometimes write $\hat{\Gamma}(P^0, k)$, instead of $\hat{\Gamma}(P^0, |\mathbf{k}|)$, where no confusion will arise. Operators that have Dirac matrix indices will be denoted by a caret; for example, $\hat{\Gamma}_{\alpha\beta}(P^0, |\mathbf{k}|)$ is such an operator.]

The reduction from four dimensions to three is achieved by restricting k^0 in some fashion. One possibility is to take $k^0 = 0$. Another option is to follow Gross and Milana [7,8] and assume that the only important singularities (for complex k^0) are those poles of the quark propagators that appear in the low-half k^0 plane. The first pole, at $k^0 = -P^0/2 + E(\mathbf{k}) - i\epsilon$, has the quark on its *positive* mass shell. The second singularity has the antiquark on its *negative* mass shell: $k^0 = P^0/2 + E(\mathbf{k}) - i\epsilon$. (The three-dimensional integral associated with the residue of the second pole has no singularity.) In general, the residue of the first pole appears in the three-dimensional integral equation for $\hat{\Gamma}(P^0, |\mathbf{k}|)$, a vertex function which exhibits a cut in the P^0 variable for $P^0 > 2m_q$. Here we will demonstrate that this cut is absent (or negligible), if the long-range potential is "confining."

In Fig. 2(b), we indicate the kind of coupled equations for the vertex functions that arise in the Gross-Milana scheme. (We recall that, since those authors were studying meson *bound states*, their equations have no driving term.) In Fig. 2(b), the crosses denote on-mass-shell quarks, or antiquarks on their negative mass shell. The crosses on the quark lines specify that $k_0 = -P_0/2 + E(\mathbf{k})$, or $k'_0 = -P_0/2 + E(\mathbf{k}')$. The crosses on the antiquark lines specify that $k_0 = P_0/2 + E(\mathbf{k})$ or $k'_0 = P_0/2 + E(\mathbf{k}')$, etc. With reference to Fig. 2(b), we remark that, after performing the integration over k'_0, we have coupled equations for two vertex functions, one with the quark on-mass-shell and the other with the antiquark on its negative mass shell [7,8]. Gross and Milana have shown that the coupling terms in these equations are small if the quarks have large masses. For pseudoscalar bound states and for the light up and down quarks, the coupling terms are also rather small, except in the case of the pion. If we drop the coupling terms we have an equation of the form shown in Fig. 3.

To further motivate this work, we note that the bosonization of the flavor-SU(2) NJL model yields a scalar-isoscalar (sigma) meson, with $m_\sigma^2 = (2m_q)^2 + m_\pi^2$ [5,9]. This state is strongly coupled to the two-π continuum and we have been interested in its fate when the coupling to the two-π continuum is taken into account [5]. In Fig. 4(a) we indicate the mean-field term in the σ

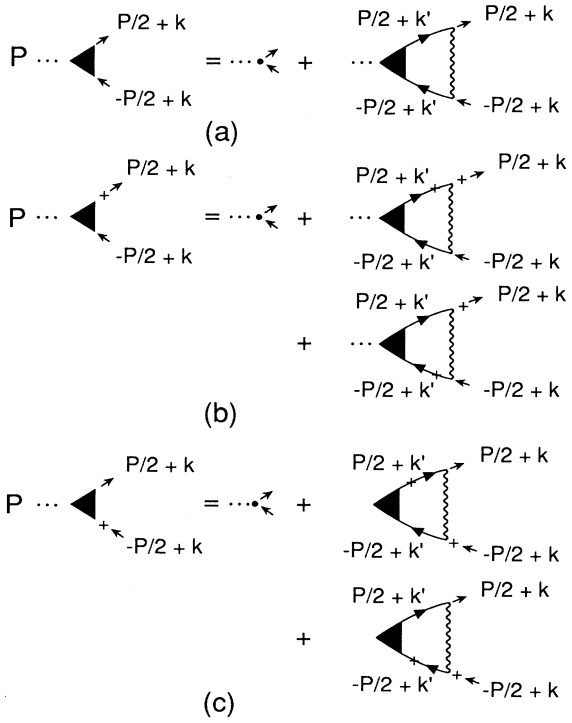

FIG. 2. (a) Representation of the four-dimensional integral equation for the scalar-isoscalar vertex $\hat{\Gamma}_{\alpha\beta}(P^2, P\cdot k, k^2)$. The wavy line denotes the interaction and the filled triangle is the vertex. (b) and (c) Integral equations for the vertex with either the quark on its positive mass-shell, or with the antiquark on its negative mass shell [7,8]. In (b) we have $k^0 = -P^0/2 + E(\mathbf{k})$, and in (c) we have $k^0 = P^0/2 + E(\mathbf{k})$.

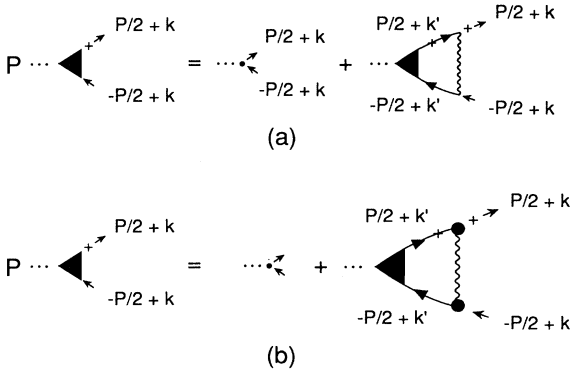

FIG. 3. (a) Schematic representation of an equation for the vertex, with the quark on its positive mass shell. Here $k^0 = -P^0/2 + E(\mathbf{k})$, and $k'^0 = -P^0/2 + E(\mathbf{k})$. (b) Inclusion of form factors (filled circles) that improve convergence of the equation shown in (a). (See the discussion in Ref. [8].)

self-energy and the contribution to the σ self-energy to one-loop order. In Fig. 4(a), we also show a correction to the self-energy due to coupling to states of the two-pion continuum. We can calculate the imaginary part of that self-energy contribution for $4m_\pi^2 < P^2 < 4m_q^2$ [5]. However, for $P^2 > 4m_q^2$ we encounter the singularities of the quark-loop integrals [5]. We suggest that the calculation may be carried out for $P^2 > 4m_q^2$, if we insert the appropriate vertex, $\hat{\Gamma}(P^0, |k|)$, as indicated in Fig. 4(b). Once the imaginary part of the last diagram in Fig. 4(b) is calculated, one can obtain the real part *via* a dispersion relation where only physical (hadron) cuts appear. That program was developed, in some detail, in Refs. [2,3,10].

As stated earlier, we will consider reduction schemes that lead to a three-dimensional integral equation for $\hat{\Gamma}(P^0, |\mathbf{k}|)$. In the first, and simplest of these schemes, we will replace the quark-antiquark propagators by another propagator that fixes $k_0 = k_0' = 0$, while maintaining the same right-hand (unitarity) cut as that obtained from the Feynman propagators. (See Sec. II.) In that approximation, we will find that we can study an integral equation for a *single* function, of two variables, while, in general, one has four functions of three variables to consider:

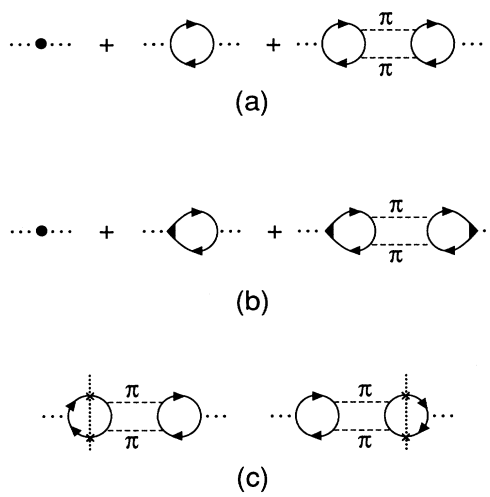

FIG. 4. (a) Schematic representation of the self-energy of the σ field of the bosonized NJL model [2,6]. The first term is the mean-field result. The first plus the second term gives $m_\sigma^2 = 4m_q^2 + m_\pi^2$. The third term arises when we consider the coupling of the σ field to the two-pion continuum at one-loop order [5]. The second and third diagrams give rise to cuts when $P^2 > 4m_q^2$. The third diagram also has a cut for $P^2 > 4m_\pi^2$, corresponding to on-mass-shell pions. (b) Inclusion of vertex functions in the calculation of the diagrams of (a). (c) An example of a discontinuity associated with the quark and antiquark being on-mass shell that is absent for a confining interaction. Here the crosses denote a quark and antiquark on their positive mass shells. (This diagram has an additional cut starting at $P^2 = 16m_q^2$ that we do not consider in this work, since $P^0 < 4m_q$ here.)

$$\hat{\Gamma}(P^2, P\cdot k, k^2) = \Gamma_1(P^2, P\cdot k, k^2) + \not{P}\Gamma_2(P^2, P\cdot k, k^2) + \not{k}\Gamma_3(P^2, P\cdot k, k^2) + \not{P}\not{k}\Gamma_4(P^2, P\cdot k, k^2), \tag{1.5}$$

where

$$\hat{k}^\mu \equiv k^\mu - \frac{(k\cdot P)P^\mu}{P^2}. \tag{1.6}$$

We may call the representation presented in Eq. (1.5) the "covariant representation." The use of $\hat{\not{k}}$ rather than $\not{k}$ in Eq. (1.5) is useful when performing various trace operations in order to obtain coupled equations for the functions $\Gamma_i(P^2, P\cdot k, k^2)$, or the functions $\Gamma_i(P^0, |\mathbf{k}|)$.

For the purposes of this work, we define

$$k_{\rm on}^2 = (P^0)^2/4 - m_q^2, \tag{1.7}$$

which is positive for $P^0 > 2m_q$. Therefore, we will write $\Gamma(k_{\rm on}, |\mathbf{k}|)$ or $\Gamma(k_{\rm on}, k)$, in some cases, instead of $\Gamma(P^0, |\mathbf{k}|)$. Note that, for $P^0 > 2m_q$, $k_{\rm on} = [(P^0)^2/4 - m_q^2]^{1/2}$ is the magnitude of the quark momenta in the center-of-mass frame. (In the absence of confinement, quarks of momentum of magnitude $k_{\rm on}$ can propagate to infinite distances.)

In Sec. II, we describe the first of our reduction schemes. That scheme is most appropriate for a problem where pair currents are not important, so that the quarks and the antiquarks may be represented by the Dirac spinors $u(\mathbf{k}, s_1), v(-\mathbf{k}, s_2)$, respectively. After we see how the model performs in that case, we go on to study equations, analogous to those investigated by Gross and Milana, in Sec. III. As noted by those authors, in passing from a nonrealativistic formulation of a bound-state equation to a relativistic formulation, some convergence factors are lost in the (reduced) three-dimensional relativistic integral equation. Therefore, one needs to consider a procedure for insuring convergence. [See Fig. 3(b).] In Sec. IV, we use the vertex function obtained in Sec. II to see how $J_S(P^2)$ of Eq. (1.4) is modified, if we insert that vertex function when evaluating the quark-loop integral that defines $J_S(P^2)$. In Sec. IV we develop a representation of the vertex using positive- and negative-energy (Dirac) projection operators. We find that this representation yields coupled equations that have well-behaved solutions, and some of these solutions are exhibited. Section V contains some further discussion and some conclusions. Finally, in the Appendix we show how our momentum-space equation leads to a vertex that vanishes when both particles go on to their positive mass shell. This property is related to the infrared behaviour of the confining potential, as is to be expected.

Before entering our general discussion, it is worth pointing out that, for convenience in our numerical analysis, we have used a potential of the form $V(r) = \kappa r e^{-\mu r}$. (See Sec. III.) For the parameters chosen, $V(r)$ has a maximum value of about 1.5 GeV. However, for the energies of concern in our work (P^0 <1 GeV), $V(r)$ acts very much like the linear potential $V = \kappa r$. Therefore, our vertex functions behave like vertex functions for a linear potential for the values of P^0 considered here.

II. USE OF PROJECTION OPERATORS IN THE CALCULATION OF VERTEX FUNCTIONS

Let us introduce the standard projection operators

$$\Lambda^{(+)}(\mathbf{k}) = \frac{\not{k} + m_q}{2m_q} , \tag{2.1}$$

and

$$\Lambda^{(-)}(-\mathbf{k}) = \frac{\tilde{\not{k}} + m_q}{2m_q} , \tag{2.2}$$

where $k^\mu = (E(\mathbf{k}), \mathbf{k})$ and $\tilde{k}^\mu = (-E(\mathbf{k}), \mathbf{k})$.

Now consider the case where k_0 is fixed by some prescription. In that case we may write, for $\mathbf{P} = 0$,

$$\hat{\Gamma}(P^0, |\mathbf{k}|) = \Gamma_1(P^0, |\mathbf{k}|) + \not{P}\Gamma_2(P^0, |\mathbf{k}|) + \hat{\not{k}}\Gamma_3(P^0, |\mathbf{k}|) + \not{P}\hat{\not{k}}\Gamma_4(P^0, |\mathbf{k}|). \tag{2.3}$$

If we consider the projected operator, $\Lambda^{(+)}(\mathbf{k})\hat{\Gamma}(P^0, |\mathbf{k}|)\Lambda^{(-)}(-\mathbf{k})$, we find

$$\Lambda^{(+)}(\mathbf{k})\hat{\Gamma}(P^0, |\mathbf{k}|)\Lambda^{(-)}(-\mathbf{k}) = \Gamma(P^0, |\mathbf{k}|)\Lambda^{(+)}(\mathbf{k})\Lambda^{(-)}(-\mathbf{k}), \tag{2.4}$$

where $\Gamma(P^0, |\mathbf{k}|)$ is a linear combination of three of the four functions appearing in Eq. (2.3):

$$\Gamma(P^0, |\mathbf{k}|) = \Gamma_1(P^0, |\mathbf{k}|) + m_q\Gamma_3(P^0, |\mathbf{k}|) + P^0E(\mathbf{k})\Gamma_4(P^0, |\mathbf{k}|). \tag{2.5}$$

In this section we will write an equation for the function $\Gamma(P^0, |\mathbf{k}|)$ that is defined in Eqs. (2.4) and (2.5). It is important to note that $\Gamma(P^0, k_{\rm on})$, which is the value of $\Gamma(P^0, |\mathbf{k}|)$ of Eq. (2.5) when $|\mathbf{k}| = k_{\rm on}$, appears when calculating the part of a diagram where *both* quark and antiquark go on their *positive* mass shells. For *confining* potentials, we have $\Gamma(P^0, k_{\rm on}) = 0$.

The motivation for considering the projected vertex operator becomes clear when we consider reduction schemes implemented for the four-dimensional equation satisfied by $\hat{\Gamma}_{\alpha\beta}(P, k) = \hat{\Gamma}_{\alpha\beta}(P^2, P\cdot k, k^2)$. We have, in the case the interaction does not contain Dirac or isospin matrices, the four-dimensional equation

$$\hat{\Gamma}(P, k) = 1 + \int \frac{d^4k'}{(2\pi)^4} iS(P/2 + k')\hat{\Gamma}(P, k') \times iS(-P/2 + k')[-iV(k, k')]. \tag{2.6}$$

[See Fig. 2(a).]

One of the often used, standard reductions of such an equation proceeds by replacing the product of Feynman Green's functions by a Green's function that has the same right-hand (unitarity) cut and that restricts the value of k_0 and k_0' in some fashion. In case the potential does not contain Dirac matrices, we have

$$\hat{\Gamma}(P, k) = 1 + \int d^4k' V(k, k')\tilde{g}(P, k') \times \Lambda_1^{(+)}(\mathbf{k}')\hat{\Gamma}(P, k')\Lambda_2^{(-)}(-\mathbf{k}'), \tag{2.7}$$

where $\tilde{g}(P, k') = \delta(k'^0)g(P, k')$, with

$$g(P, k') = \frac{1}{(2\pi)^3}\left[\frac{m_q}{E(\mathbf{k}')}\right]^2 \frac{1}{[P^0 - 2E(\mathbf{k}') + i\epsilon]} \tag{2.8}$$

representing one possible choice for $\tilde{g}$. Note that the reduced propagator of Eq. (2.8) is a member of an infinite class of propagators that lead to the same right-hand (unitarity) cut as the Feynman propagators of the original equation, Eq. (2.5).

The extension to the case where the potential contains Dirac matrices and isospin matrices is straightforward. In the general case, Eq. (2.5) becomes

$$\hat{\Gamma}(P, k) = 1 + i\int \frac{d^4k'}{(2\pi)^4} O^i(1)S(P/2 + k')\hat{\Gamma}(P, k') \times S(-P/2 + k')O^i(2)V_i(k, k'), \tag{2.9}$$

where a sum over i is implied. Here, we have introduced an interaction of the form [7,8]

$$\hat{V}(k, k') = \sum_i O^i(1)O^i(2)V_i(k, k'), \tag{2.10}$$

where $O^i(1)$ and $O^i(2)$ are Dirac or isospin matrices associated with the quark and antiquark vertices. [If desired, we can replaced $V_i(k, k')$ by a single function, $V(k, k')$, in Eqs. (2.9) and (2.10).]

For example, here we will study the form

$$\hat{V}(k, k') = K(\Delta^2)[1 - \gamma_5(1)\gamma_5(2)\boldsymbol{\tau}_1\cdot\boldsymbol{\tau}_2], \tag{2.11}$$

with $\Delta^2 = (\mathbf{k} - \mathbf{k}')^2$. (As before, the index 1 refers to the quark and the index 2 refers to the antiquark.) The analysis proceeds by multiplying Eq. (2.6) by $\Lambda_1^{(+)}(\mathbf{k})$ on the left and by $\Lambda_2^{(-)}(-\mathbf{k})$ on the right, and then performing a trace operation. The following functions appear:

$$a(k) = \tfrac{1}{4}\mathrm{Tr}[\Lambda_1^{(+)}(\mathbf{k})\Lambda_2^{(-)}(-\mathbf{k})] = -\frac{\mathbf{k}^2}{2m_q^2}, \tag{2.12}$$

and

$$b(\mathbf{k}, \mathbf{k}') = \tfrac{1}{4}\mathrm{Tr}\{\Lambda_1^{(+)}(\mathbf{k})\Lambda_1^{(+)}(\mathbf{k}')\Lambda_2^{(-)}(-\mathbf{k}')\Lambda_2^{(-)}(-\mathbf{k}) - 3[\Lambda_1^{(+)}(\mathbf{k})\gamma_5\Lambda_1^{(+)}(\mathbf{k}')\Lambda_2^{(-)}(-\mathbf{k}')\gamma_5\Lambda_2^{(-)}(-\mathbf{k})]\} \tag{2.13}$$

$$= -\frac{1}{2m_q^4}(\mathbf{k}^2\mathbf{k}'^2) + \left[\frac{E(\mathbf{k})E(\mathbf{k}') - 2m_q^2}{2m_q^4}\right](\mathbf{k}\cdot\mathbf{k}'). \tag{2.14}$$

[The factor of 3 in Eq. (2.13) is an isospin factor.]

Finally, we arrive at the equation for the (single) function, $\Gamma(P^0, |\mathbf{k}|)$:

$$\Gamma(P^0, |\mathbf{k}|) = 1 + \int d|\mathbf{k}'|U(|\mathbf{k}|, |\mathbf{k}'|)\frac{\Gamma(P^0, |\mathbf{k}'|)}{P^0 - 2E(\mathbf{k}') + i\epsilon}, \tag{2.15}$$

where

$$U(|\mathbf{k}|,|\mathbf{k}'|)=\frac{1}{(2\pi)^3}\left[\frac{m_q}{E(\mathbf{k}')}\right]^2\frac{\mathbf{k}'^2}{a(\mathbf{k})}\int d\Omega_{\mathbf{k}'}K(\Delta^2)b(\mathbf{k},\mathbf{k}'). \tag{2.16}$$

In Eq. (2.16), $d\Omega_{\mathbf{k}'}$ denotes the solid angle for the vector $\mathbf{k}'$. To proceed further, we need to specify the form of $K(\Delta^2)$ appearing in Eq. (2.11). That is done in the next section.

III. POTENTIAL MODEL FOR CONFINEMENT AND NUMERICAL RESULTS

Here, we follow the work of other authors [7,8] and consider a coordinate-space potential of the form

$$V_L(\mathbf{r})=\kappa r e^{-\mu r}. \tag{3.1}$$

We note that, if μ is small enough, Eq. (3.1) represents a linear potential over a range of several fermis. Usually, taking $\mu\simeq 0.050$ GeV is adequate. The advantage of using Eq. (3.1) is that finite values of μ regulate the strong singularities at $\mathbf{k}=0$ of the Fourier transform of $V_L(\mathbf{r})$. (There is no particular advantage gained in going to the limit where μ is made very much smaller.)

If we use the potential of Eq. (3.1), we have

$$K(\Delta^2)=4\pi\kappa\left\{-\frac{2}{(\Delta^2+\mu^2)^2}+\frac{8\mu^2}{(\Delta^2+\mu^2)^3}\right\} \tag{3.2}$$

with $\Delta^2=(\mathbf{k}-\mathbf{k}')^2$.

Note that Δ^2 does not describe energy transfer. If we had placed the quark on-mass shell, rather than specifying $k^0=0$, we would have $\Delta^2=-[E(\mathbf{k})-E(\mathbf{k}')]^2+(\mathbf{k}-\mathbf{k}')^2$. As discussed by Gross and Milana [7,8], allowing for energy transfer worsens the convergence properties of the integral equation and requires the insertion of form factors, as in Fig. 3(b). We have not considered that option here.

With this specification of $K(\Delta^2)$, we can complete the integration over angles in Eq. (2.16). We have

$$U(|\mathbf{k}|,|\mathbf{k}'|)=-\frac{\kappa}{\pi}\left[\frac{m_q^2}{E^2(\mathbf{k}')}\right]\left(\frac{\mathbf{k}'^2}{\mathbf{k}^2}\right)\{aA_{02}+bA_{03}+cA_{12}+dA_{13}\}, \tag{3.3}$$

where

$$A_{nm}(z)=\int_{-1}^{1}\frac{t^n dt}{(t-z)^m}, \tag{3.4}$$

$$z=\frac{\mathbf{k}^2+\mathbf{k}'^2+\mu^2}{2|\mathbf{k}||\mathbf{k}'|}>1, \tag{3.5}$$

and

$$a=1/(2m_q^2), \tag{3.6}$$

$$b=\mu^2/(m_q^2|\mathbf{k}||\mathbf{k}'|), \tag{3.7}$$

$$c=[2m_q^2-E(\mathbf{k})E(\mathbf{k}')]/(2|\mathbf{k}||\mathbf{k}'|m_q^2), \tag{3.8}$$

$$d=\mu^2[2m_q^2-E(\mathbf{k})E(\mathbf{k}')]/(m_q^2\mathbf{k}^2\mathbf{k}'^2). \tag{3.9}$$

Note that the A_{ij} are singular as $z\to 1$:

$$A_{02}(z)=\frac{2}{z^2-1}, \tag{3.10}$$

$$A_{03}(z)=-\frac{2z}{(z^2-1)^2}, \tag{3.11}$$

$$A_{12}(z)=\ln\left(\frac{z-1}{z+1}\right)+\frac{2z}{z^2-1}, \tag{3.12}$$

and

$$A_{13}(z)=-\frac{2}{(z^2-1)^2}. \tag{3.13}$$

We have obtained solutions of Eq. (2.15) for the case $m_q=0.33$ GeV, $\mu=0.05$ GeV, and $\kappa=0.30$ GeV^2. Values of $\Gamma(P^0,|\mathbf{k}|)$, for several values of P^0, are shown in Fig. 5. In the absence of confinement, the threshold for the appearance of free quarks is $P^0=2m_q$, which is $P^0=0.66$ GeV in this case. We see in Fig. 5, that for $P^0>0.66$ GeV, $\Gamma(P^0,|\mathbf{k}|)$ has zeroes. These zeros appear when $|\mathbf{k}|=k_{\rm on}$. In addition, we see a significant reduction of $\Gamma(P^0,|\mathbf{k}|)$ for small $|\mathbf{k}|$. [The asymptotic value of unity is approached for all $|\mathbf{k}|$, if P^0 is large enough, since our confining potential has a *finite* maximum value of several GeV. For $\kappa=0.30$ GeV^2 and $\mu=0.050$ GeV, the maximum value of the potential is $(\kappa/\mu)e^{-1}$=2.2 GeV at $r=\mu^{-1}$=4 fm.] In Sec. V, we will continue our analysis based upon the use of the positive- and negative-energy projection operators. However, in the next section, we first comment on the use of vertex functions for confining potentials when developing a generalized NJL model.

IV. DESCRIPTION OF CONFINEMENT IN A GENERALIZED NAMBU–JONA-LASINIO MODEL

In this section we will apply the results represented in Fig. 5 to calculate $J_S'(P^2)$. [See Fig. 1(b)]. This application requires a further approximation. The quark and antiquark are on their positive mass shells in the calculation of the imaginary part of $J_S'(P^2)$. However, in the calculation of the real part of $J_S'(P^2)$ the quark or antiquark can be found off-shell. Thus, the use of $\Gamma(P^0,|\mathbf{k}|)$, taken from Fig. 5, as the vertex shown in Fig. 1(b), requires the assumption that we may use $\Gamma(P^0,|\mathbf{k}|)$ in the larger space of Dirac matrices, without making a serious error. At this point, the use of the vertex obtained from the reduced (pair-suppressed) equations in a *full* Dirac space is part of our model building effort. We are interested in exhibiting the results of this approximation in this section.

Recall that, in the NJL model, considered at one-loop order, one finds a scalar (σ) boson, whose mass is obtained from the equation

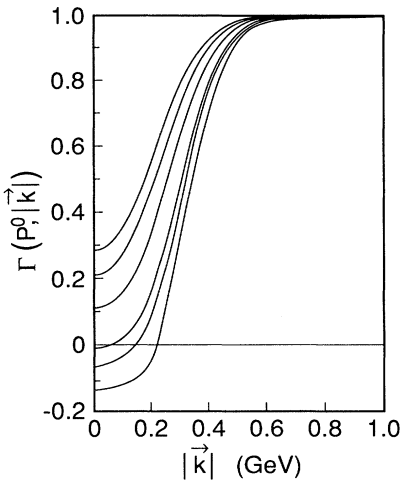

FIG. 5. Values of $\Gamma(P^0,|\mathbf{k}|)$, defined in Eqs. (2.4) and (2.5), are given as a function of $|\mathbf{k}|$ for several values of P^0. Here $m_q = 0.33$ GeV, $\mu = 0.050$ GeV, and $\kappa = 0.30$ GeV^2. The values of P^0 and $k_{\rm on}$ are (a) $P^0 = 0.10$ GeV; (b) $P^0 = 0.30$ GeV; (c) $P^0 = 0.50$ GeV; (d) $P^0 = 0.67$ GeV, $k_{\rm on} = 0.057$ GeV; (e) $P^0 = 0.72$ GeV, $k_{\rm on} = 0.144$ GeV; (f) $P^0 = 0.80$ GeV, $k_{\rm on} = 0.226$ GeV; with $P^0 = 0.10$ GeV corresponding to the uppermost curve, etc. [Note that for $P^0 > 2m_q$, we have $\Gamma(P^0,k_{\rm on}) = \Gamma(k_{\rm on},k_{\rm on}) = 0$.] The potential used for these calculations is given in Eq. (2.11).

$$1 - G_S J_S(P^2) = 0. \tag{4.1}$$

A solution exists for $P^2 = m_\sigma^2$, where $m_\sigma^2 = 4m_q^2 + m_\pi^2$, as noted above. This feature may be seen from inspection of Fig. 6, where the dashed line represents $\mathrm{Re}J_S(P^2)$ and the dotted line is $\mathrm{Im}J_S(P^2)$. [Note that $\mathrm{Im}J_S(P^2)$ is nonzero for $P^2 > 4m_q^2$.] The light horizontal line denotes

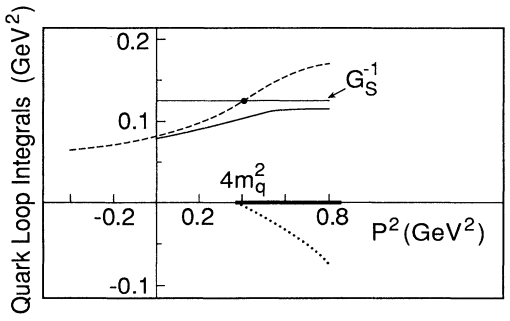

FIG. 6. The dashed line shows the value of $\mathrm{Re}J_S(P^2)$, while the dotted line shows $\mathrm{Im}J_S(P^2)$. Here we took $m_q = 302$ MeV and used a cutoff on the magnitude of the integration variable: $|\mathbf{k}| \leq \Lambda_3$, where $\Lambda_3 = 0.703$ GeV. [See Fig. 1(a) and Eq. (1.3).] The light horizontal line represents G_S^{-1} and the other solid line is $J'_S(P^2)$. [See Eq. (4.2).] Note that $\mathrm{Im}J'_S(P^2) = 0$. The intersection of the dashed line with the light horizontal line $(1/G_S)$ determines the solution of the equation $1 - G_S J_S(P^2) = 0$, at $P^2 = m_\sigma^2$.

the value of G_S^{-1}. The intersection of the dashed line with the line representing G_S^{-1} is the point where $P^2 = m_\sigma^2$ and represents a solution of Eq. (4.1). Note that the σ boson mass is slightly above the threshold for the two-quark continuum.

In Fig. 6, the solid line is the result for $J'_S(P^2)$, calculated using the vertex functions of Fig. 5. That is,

$$-iJ'_S(P^2) = (-1)n_c n_f \mathrm{Tr}\int \frac{d^4k}{(2\pi)^4} iS(P/2+k)\Gamma(P^0,|\mathbf{k}|) \times iS(-P/2+k). \tag{4.2}$$

We may make several important observations upon inspecting Fig. 6. First, $\mathrm{Im}J'_S(P^2) = 0$ everywhere (including the region $P^2 > 4m_q^2$). Second, there is no longer a prediction of a low-mass *physical* σ meson. That follows from the absence of solutions of the equation $1 - G_S J'_S(P^2) = 0$. Further, we see that the values of $J_S(P^2)$ and $J'_S(P^2)$ are very similar for $P^2 \simeq 0$.

In our early work, we have shown that, even in the presence of a two-pion continuum that is strongly coupled to the scalar-isoscalar $q\bar{q}$ states, a sigma-dominance model provides an accurate representation of the dynamics for $P^2 \leq 0$ [10]. Because of the near identity of $J'_S(P^2)$ and $J_S(P^2)$ for $P^2 \lesssim 0$, many of the results obtained using the original NJL model will be unmodified. For example, if we consider the calculation of the nucleon σ term using a σ-dominance model, within the context of the NJL model [11], there appears an enhancement factor of $[1 - G_S J_S(0)]^{-1}$. That factor would now be $[1 - G_S J'_S(0)]^{-1}$, which differs little from $[1 - G_S J_S(0)]^{-1}$. Therefore, the results of Ref. [11] are still useful in the case of our generalized NJL model.

To understand further the utility of studying the vertex of the confining field, we present an expression for the scalar-isoscalar hadronic current correlator [see Eq.(1.1)] derived in Ref. [2]. We find

$$C_S(P^2) = \frac{J'_S(P^2) + K'_S(P^2)}{1 - G_S[J'_S(P^2) + K'_S(P^2)]}. \tag{4.3}$$

Here $J'_S(P^2)$ was defined in Eq. (4.2), while $K'_S(P^2)$ is calculated from the diagram on the right-hand side of Fig. 4(b). (In Ref. [2], $J'_S(P^2)$ and $K'_S(P^2)$ are denoted as $\hat{J}_S(P^2)$ and $\hat{K}_S(P^2)$.) It may be seen that $C_S(P^2)$ only has cuts starting at $P^2 = 4m_\pi^2$, since the inclusion of the vertex function for the confining field eliminates the $q\bar{q}$ unitarity cuts.

The rather complex situation that emerges in the study of the scalar-isoscalar correlator is described in Ref. [10]. A simpler case is the study of the vector-isovector correlator [2]. There, an equation analogous to Eq. (4.3) is derived

$$C_{(\rho)}(P^2) = \frac{J'_{(\rho)}(P^2) + K'_{(\rho)}(P^2)}{1 - G_V[J'_{(\rho)}(P^2) + K'_{(\rho)}(P^2)]}. \tag{4.4}$$

This expression may be put into the form

$$C_{(\rho)}(P^2) = J'_{(\rho)}(P^2) + \tilde{C}_{(\rho)}(P^2) \tag{4.5}$$

and it is seen that $\tilde{C}_{(\rho)}(P^2)$ exhibits a resonant structure due to the formation of the rho meson, while $J'_{(\rho)}(P^2)$ is a smooth function [2]. Again, $C_{(\rho)}(P^2)$ has no $q\bar{q}$ unitarity cut and satisfies physically meaningful dispersion relations. (Note that $J'_{(\rho)}(P^2)$ and $K'_{(\rho)}(P^2)$ are denoted as $\hat{J}_{(\rho)}(P^2)$ and $\hat{K}_{(\rho)}(P^2)$ in Ref. [2]. In that work the full tensor structure of the correlator, $C^{\mu\nu}_{(\rho)}(P^2)$, is given.)

V. CALCULATION OF VERTEX FUNCTIONS WITH THE USE OF PROJECTION OPERATORS

The various difficulties we have encountered in the use of the covariant representation leads us to continue our development based upon the use of the positive- and negative-energy projection operators of Eqs. (2.1) and (2.2). For the scalar-isoscalar vertex, we define

$$\Lambda^{(+)}(\mathbf{k})\hat{\Gamma}(P^2, P\cdot k, k^2)\Lambda^{(+)}(\mathbf{k}) = \Lambda^{(+)}(\mathbf{k})\Lambda^{(+)}(\mathbf{k})\Gamma^{++}(P^2, P\cdot k, k^2), \tag{5.1}$$

$$\Lambda^{(+)}(\mathbf{k})\hat{\Gamma}(P^2, P\cdot k, k^2)\Lambda^{(-)}(-\mathbf{k}) = \Lambda^{(+)}(\mathbf{k})\Lambda^{(-)}(-\mathbf{k})\Gamma^{+-}(P^2, P\cdot k, k^2), \tag{5.2}$$

$$\Lambda^{(-)}(-\mathbf{k})\hat{\Gamma}(P^2, P\cdot k, k^2)\Lambda^{(+)}(\mathbf{k}) = \Lambda^{(-)}(-\mathbf{k})\Lambda^{(+)}(\mathbf{k})\Gamma^{-+}(P^2, P\cdot k, k^2), \tag{5.3}$$

$$\Lambda^{(-)}(-\mathbf{k})\hat{\Gamma}(P^2, P\cdot k, k^2)\Lambda^{(-)}(-\mathbf{k}) = \Lambda^{(-)}(-\mathbf{k})\Lambda^{(-)}(-\mathbf{k})\Gamma^{--}(P^2, P\cdot k, k^2). \tag{5.4}$$

If we extend the procedures used in Sec. II, we may write coupled equations for the functions that appear in on the right-hand sides of Eqs. (5.2) and (5.3). We put $\mathbf{P} = 0$ and again use the approximation of evaluating the k'_0 integrals by closing the contour in the lower-half plane and picking up only the residues of the Green's function poles. We find that Γ^{+-} is only coupled to Γ^{-+} and that Γ^{++} and Γ^{--} may be determined from the knowledge of Γ^{+-} and Γ^{-+}. We also find that the interaction terms do not contain P^0, which now only appears in the energy denominators.

The equations obtained in the projection operator scheme, in the absence of retardation, are

$$\begin{bmatrix} \Gamma^{+-}(P^0, |\mathbf{k}|) \\ \Gamma^{-+}(P^0, |\mathbf{k}|) \end{bmatrix} = \begin{bmatrix} 1 \\ 1 \end{bmatrix} + \int \frac{d\mathbf{k}'}{(2\pi)^3} V(\mathbf{k}-\mathbf{k}')t(\mathbf{k},\mathbf{k}') \times \begin{bmatrix} \Gamma^{+-}(P^0, |\mathbf{k}'|) \\ \Gamma^{-+}(P^0, |\mathbf{k}'|) \end{bmatrix}, \tag{5.5}$$

where the matrix $t(\mathbf{k},\mathbf{k}')$ is

$$t(\mathbf{k},\mathbf{k}') = \begin{bmatrix} \dfrac{A(\mathbf{k},\mathbf{k}')}{P^0 - 2E(\mathbf{k}') + i\epsilon} & \dfrac{B(\mathbf{k},\mathbf{k}')}{P^0 + 2E(\mathbf{k}')} \\ -\dfrac{B(\mathbf{k},\mathbf{k}')}{P^0 - 2E(\mathbf{k}') + i\epsilon} & -\dfrac{A(\mathbf{k},\mathbf{k}')}{P^0 + 2E(\mathbf{k}')} \end{bmatrix} \tag{5.6}$$

Here,

$$A(\mathbf{k},\mathbf{k}') = \frac{1}{2E^2(\mathbf{k}')}\left[-\mathbf{k}'^2 + \frac{\mathbf{k}\cdot\mathbf{k}'}{\mathbf{k}^2}(E(\mathbf{k})E(\mathbf{k}') + m_q^2)\right] \tag{5.7}$$

and

$$B(\mathbf{k},\mathbf{k}') = \frac{1}{2E^2(\mathbf{k}')}\left[\mathbf{k}'^2 + \frac{(\mathbf{k}\cdot\mathbf{k}')}{\mathbf{k}^2}(E(\mathbf{k})E(\mathbf{k}') - m_q^2)\right]. \tag{5.8}$$

The transparent aspect of these equations clearly demonstrates the advantage of the projection operator approach.

We now consider scalar confinement and make use of the interaction of Eqs. (3.1) and (3.2). We define

$$a_0(|\mathbf{k}|, |\mathbf{k}'|) = \int d\Omega_{\mathbf{k}'} K(\Delta^2) \tag{5.9}$$

$$= -32\pi^2\kappa\left\{\frac{1}{x^2 - y^2} - \frac{4\mu^2 x}{(x^2-y^2)^2}\right\}, \tag{5.10}$$

where

$$x = \mathbf{k}^2 + \mathbf{k}'^2 + \mu^2, \tag{5.11}$$

and

$$y = 2|\mathbf{k}||\mathbf{k}'|. \tag{5.12}$$

We also need

$$a_1(|\mathbf{k}|, |\mathbf{k}'|) = \int d\Omega_{\mathbf{k}'} K(\Delta^2)(\hat{\mathbf{k}}\cdot\hat{\mathbf{k}}') \tag{5.13}$$

$$= \frac{1}{y}[x a_0 - b_1], \tag{5.14}$$

where

$$b_1 = 16\pi^2\kappa\left\{\frac{1}{y}\ln\frac{x-y}{x+y} + \frac{8\mu^2}{x^2-y^2}\right\}. \tag{5.15}$$

Thus, Eq (5.5) may be written

$$\begin{bmatrix} \Gamma^{+-}(P^0), |\mathbf{k}|) \\ \Gamma^{-+}(P^0, |\mathbf{k}|) \end{bmatrix} = \begin{bmatrix} 1 \\ 1 \end{bmatrix} + \int d|\mathbf{k}'|h(\mathbf{k},\mathbf{k}') \begin{bmatrix} \Gamma^{+-}(P^0, |\mathbf{k}'|) \\ \Gamma^{-+}(P^0, |\mathbf{k}'|) \end{bmatrix}, \tag{5.16}$$

where the matrix $h(\mathbf{k},\mathbf{k}')$ is

$$h(\mathbf{k},\mathbf{k}') = \begin{bmatrix} \dfrac{\alpha(\mathbf{k},\mathbf{k}')}{P^0 - 2E(\mathbf{k}') + i\epsilon} & \dfrac{\beta(\mathbf{k},\mathbf{k}')}{P^0 + 2E(\mathbf{k}')} \\ -\dfrac{\beta(\mathbf{k},\mathbf{k}')}{P^0 - 2E(\mathbf{k}') + i\epsilon} & -\dfrac{\alpha(\mathbf{k},\mathbf{k}')}{P^0 + 2E(\mathbf{k}')} \end{bmatrix} , \tag{5.17}$$

with

$$\alpha(\mathbf{k},\mathbf{k}') = \frac{1}{(2\pi)^3}\frac{\mathbf{k}'^2}{2E^2(\mathbf{k}')}\left\{-\mathbf{k}'^2 a_0 + \frac{|\mathbf{k}'|}{|\mathbf{k}|}[E(\mathbf{k})E(\mathbf{k}') + m_q^2]a_1\right\} , \tag{5.18}$$

$$\beta(\mathbf{k},\mathbf{k}') = \frac{1}{(2\pi)^3}\frac{\mathbf{k}'^2}{2E^2(\mathbf{k}')}\left\{\mathbf{k}'^2 a_0 + \frac{|\mathbf{k}'|}{|\mathbf{k}|}[E(\mathbf{k})E(\mathbf{k}') - m_q^2]a_1\right\} . \tag{5.19}$$

We note that our equations take on a relatively simple form, in part, due to the neglect of retardation of the interaction. Results obtained for $\Gamma^{+-}(P^0,|\mathbf{k}|)$ and $\Gamma^{-+}(P^0,|\mathbf{k}|)$ are shown in Figs. 7 and 8. In Fig. 7, we see that $\Gamma^{+-}(P^0,k_{\rm on}) = 0$, as expected.

At this point, we can return to our calculation of $J_S(P^2)$. Previously, we had used $\Gamma(P^0,|\mathbf{k}|)$, obtained in Sec. II, to calculate $J'_S(P^2)$. (See Fig. 5.) An improved calculation is obtained by using the following form of the fermion propagator:

$$S(p) = \frac{m_q}{E(\mathbf{p})}\left\{\frac{\Lambda^{(+)}(\mathbf{p})}{p^0 - E(\mathbf{p}) + i\epsilon} - \frac{\Lambda^{(-)}(-\mathbf{p})}{p^0 + E(\mathbf{p}) - i\epsilon}\right\} . \tag{5.20}$$

We define

$$S^{(+)}(p) = \frac{m_q}{E(\mathbf{p})}\frac{\Lambda^{(+)}(\mathbf{p})}{p^0 - E(\mathbf{p}) + i\epsilon} \tag{5.21}$$

and

$$S^{(-)}(p) = -\frac{m_q}{E(\mathbf{p})}\frac{\Lambda^{(-)}(-\mathbf{p})}{p^0 + E(\mathbf{p}) - i\epsilon} , \tag{5.22}$$

so that $S(p) = S^{(+)}(p) + S^{(-)}(p)$. Note that

$$\Lambda^{(+)}(\mathbf{p}) = \sum_s u(\mathbf{p},s)\bar{u}(\mathbf{p},s) \tag{5.23}$$

and

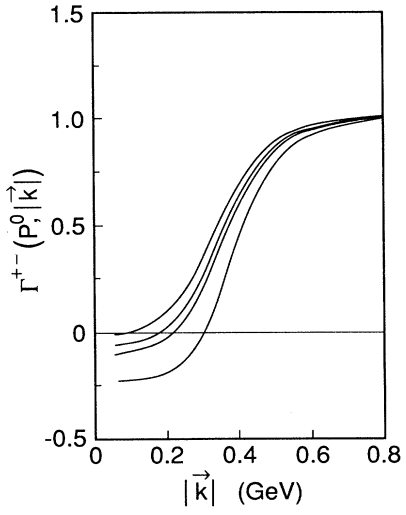

FIG. 7. Lorentz-scalar confinement. Values of $\Gamma^{+-}(P^0,|\mathbf{k}|)$ obtained from the solution of the coupled equations for Γ^{+-} and Γ^{-+} are shown. Here $m_q = 0.33$ GeV, $\mu = 0.050$ GeV, and $\kappa = 0.3$ GeV^2. (A cutoff on the magnitude of the momenta of 1.0 GeV was used.) Note that $\Gamma^{+-}(P^0,|\mathbf{k}|) \to 1$ for large $|\mathbf{k}|$ and that $\Gamma^{+-}(P^0,k_{\rm on}) = 0$. Values of P^0 and $k_{\rm on}$ are given starting with the uppermost curve: (a) $P^0 = 0.69$ GeV; $k_{\rm on} = 0.101$ GeV; (b) $P^0 = 0.76$ GeV, $k_{\rm on} = 0.188$ GeV; (c) $P^0 = 0.80$ GeV, $k_{\rm on} = 0.226$ GeV; (d) $P^0 = 0.90$ GeV, $k_{\rm on} = 0.306$ GeV.

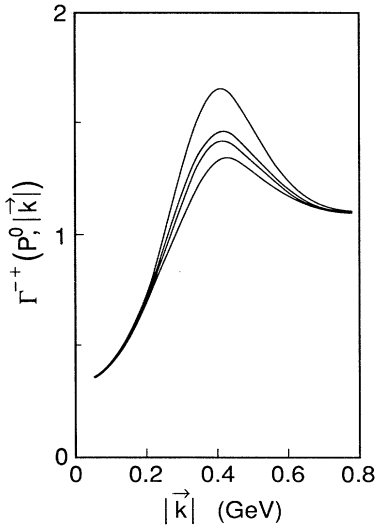

FIG. 8. Lorentz-scalar confinement. Values of $\Gamma^{-+}(P^0,|\mathbf{k}|)$ obtained from the solution of the coupled equations for Γ^{+-} and Γ^{-+} are shown. (See caption to Fig. 7.) Note that the $\Gamma^{-+}(P^0,|\mathbf{k}|)$ decrease for large $|\mathbf{k}|$, and are close to unity for $|\mathbf{k}| = 1$ GeV. Starting with the lowest curve and moving upward we have $P^0 = 0.69$ GeV, $P^0 = 0.76$ GeV, $P^0 = 0.80$ GeV, and $P^0 = 0.90$ GeV. (Corresponding values of $k_{\rm on}$ are given in the caption to Fig. 7.)

$$\Lambda^{(-)}(-\mathbf{p}) = -\sum_s v(-\mathbf{p},s)\overline{v}(-\mathbf{p},s) \ . \tag{5.24}$$

[See Eqs. (2.1) and (2.2).] With $w(\mathbf{p},s) \equiv v(-\mathbf{p},-s)$, we also may write

$$S(p) = \frac{m_q}{E(\mathbf{p})}\sum_s\left\{\frac{u(\mathbf{p},s)\overline{u}(\mathbf{p},s)}{p^0 - E(\mathbf{p}) + i\epsilon} + \frac{w(\mathbf{p},s)\overline{w}(\mathbf{p},s)}{p^0 + E(\mathbf{p}) - i\epsilon}\right\} . \tag{5.25}$$

Using Eqs. (5.18)–(5.20) in the calculation of the quark loop integral, we find that the terms $S^{(+)}(P/2+k)\Gamma^{+-}(P^0,|\mathbf{k}|)S^{(-)}(-P/2+k)$ and $S^{(-)}(-P/2+k)\Gamma^{-+}(P^0,|\mathbf{k}|)S^{(+)}(P/2+k)$ give nonzero contributions, if we again assume that the only relevant poles are those of the Green's functions in the lower-half k_0 plane. In this case, we see that Eq. (4.2) is to be replaced by

$$J_S(P^2) = in_c n_f \mathrm{Tr}\int\frac{d^4k}{(2\pi)^4}[S^{(+)}(P/2+k)\Gamma^{+-}(P^0,|\mathbf{k}|)S^{(-)}(-P/2+k)$$

$$+S^{(-)}(P/2+k)\Gamma^{-+}(P^0,|\mathbf{k}|)S^{(+)}(-P/2+k)] \tag{5.26}$$

for $\mathbf{P}=0$. The result obtained when using the values of Γ^{+-} and Γ^{-+} shown in Figs. 7 and 8 in the calculation of $J_s'(P^2)$ is shown in Fig. 9 as a solid line. For Fig. 9, we have $\kappa = 0.2$ GeV^2. We see that, here the modified vertex corresponds to a weaker repulsive effect than that obtained in the calculation exhibited in Fig. 6, where we had put $\kappa = 0.3$ GeV^2.

In other applications, we will need the values of $\Gamma^{++}(P^0,|\mathbf{k}|)$ and $\Gamma^{--}(P^0,|\mathbf{k}|)$. Using the definitions in Eqs. (5.1) and (5.4), we find

$$\Gamma^{++}(P^0,|\mathbf{k}|) = 1 + i\frac{\mathrm{Tr}}{2}\int\frac{d^4k'}{(2\pi)^4}[\Lambda^{(+)}(\mathbf{k})S^{(+)}(P/2+k')S^{(-)}(-P/2+k')\Lambda^{(+)}(\mathbf{k})\Gamma^{+-}(P^0,|\mathbf{k}|)$$

$$+\Lambda^{(+)}(\mathbf{k})S^{(-)}(P/2+k)S^{(+)}(-P/2+k)\Lambda^{(+)}(\mathbf{k})\Gamma^{-+}(P^0,|\mathbf{k}|)]V(\mathbf{k},\mathbf{k}') \tag{5.27}$$

and

$$\Gamma^{--}(P^0,|\mathbf{k}|) = 1 + i\frac{\mathrm{Tr}}{2}\int\frac{d^4k'}{(2\pi)^4}[\Lambda^{(-)}(-\mathbf{k})S^{(+)}(P/2+k')S^{(-)}(-P/2+k')\Lambda^{(-)}(-\mathbf{k})\Gamma^{+-}(P^0,|\mathbf{k}|)$$

$$+\Lambda^{(-)}(-\mathbf{k})S^{(-)}(P/2+k')S^{(+)}(-P/2+k')\Lambda^{(-)}(-\mathbf{k})\Gamma^{-+}(P^0,|\mathbf{k}|)]V(\mathbf{k},\mathbf{k}') \ . \tag{5.28}$$

Thus, once we have obtained Γ^{+-} and Γ^{-+}, we can construct Γ^{++} and Γ^{--} using the last two equations. The latter vertex functions appear when evaluating the diagram on the right in Fig. 4(b), for example.

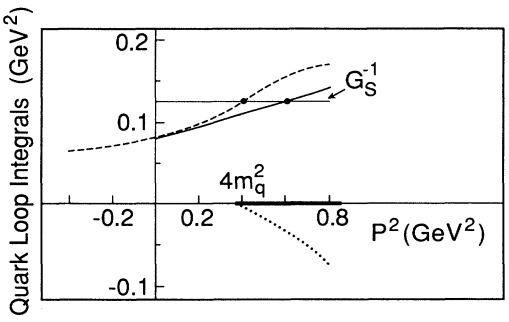

FIG. 9. The dashed line shows the value of $J_S(P^2)$, while the dotted line is $\mathrm{Im}J_S(P^2)$. [See Fig. 6.] The solid line represents the values of $J_S'(P^2)$, calculated using values of Γ^{+-} and Γ^{-+} shown in Figs. 7 and 8. Here $\kappa = 0.20$ GeV^2, $m_q = 0.302$ GeV, and $\Lambda_3 = 0.702$ GeV. [See the caption to Fig. 6.]

VI. DISCUSSION AND CONCLUSIONS

In this work, we have constructed equations for quark vertex functions for the case of a scalar-isoscalar source. We have made use of an approximate expression, Eq. (3.1), that represents a linear confining potential over the relevant kinematic range [12]. It would appear that, since in the development of the last section we only had to solve for *two* functions, Γ^{+-} and Γ^{-+}, the four equations in the covariant representation are redundant in the absence of retardation. Note that, in the absence of retardation, we have

$$\Gamma^{+-}(P^0,|\mathbf{k}|) = \Gamma_1(P^0,|\mathbf{k}|) + m_q\Gamma_3(P^0,|\mathbf{k}|) + P^0E(\mathbf{k})\Gamma_4(P^0,|\mathbf{k}|) \ , \tag{6.1}$$

$$\Gamma^{-+}(P^0,|\mathbf{k}|) = \Gamma_1(P^0,|\mathbf{k}|) + m_q\Gamma_3(P^0,|\mathbf{k}|) - P^0E(\mathbf{k})\Gamma_4(P^0,|\mathbf{k}|) \ , \tag{6.2}$$

$$\Gamma^{++}(P^0,|\mathbf{k}|) = \Gamma_1(P^0,|\mathbf{k}|) + \frac{E(\mathbf{k})}{m_q}P^0\Gamma_2(P^0,|\mathbf{k}|) - \frac{\mathbf{k}^2}{m_q}\Gamma_3(P^0,|\mathbf{k}|) \ , \tag{6.3}$$

and

$$\Gamma^{--}(P^0,|\mathbf{k}|) = \Gamma_1(P^0,|\mathbf{k}|) - \frac{E(\mathbf{k})}{m_q}P^0\Gamma_2(P^0,|\mathbf{k}|) - \frac{\mathbf{k}^2}{m_q}\Gamma_3(P^0,|\mathbf{k}|) \ , \tag{6.4}$$

In Sec. II, we based our presentation upon the use of a reduction scheme that allowed us to obtain a single three-dimensional equation from a four-dimensional equation. There are many such reduction schemes [13]; however, the particular reduction used in Sec. II is in complete correspondence with the projection operator scheme of Sec. V, if we continue to neglect energy transfer (i.e., retardation) in the interaction. For example, if we drop Γ^{-+}, and use the same interaction, we could identify $\Gamma(P^0,|\mathbf{k}|)$ of Sec. II with $\Gamma^{+-}(P^0,|\mathbf{k}|)$ of Sec. V. (The neglect of Γ^{-+} is a particularly good approximation when one considers the case of heavy quarks.)

Of particular interest is the fact that the vertex functions considered here eliminate spurious unitarity cuts in various $q\bar{q}$ amplitudes. Thus, the description of the analytic structure of these amplitudes includes only cuts due to (color-singlet) hadrons going on-mass-shell. [See Figs. 4(b) and 4(c), for example.] That feature allows us to construct dispersion relations in terms of discontinuities across *physical* cuts, as was done in Refs. [2,3,10]. We also note that, if one includes a long-range confining potential, the notion of a $q\bar{q}$ T matrix is no longer a particularly useful concept. However, in the presence of a confining interaction, we may continue to study quark correlators of the form $\langle 0|T(\bar{q}(x)q(x)\bar{q}(0)q(0))|0\rangle$, as was done in Ref. [10]. The study of the correlator is particularly simple, since the $q\bar{q}$ pair is created at a point and annihilated at another point. (In contrast, the usual calculation of a T matrix requires the presence of free quarks which converge, starting from large separations, scatter, and then separate.) In the calculation of the correlator, the $q\bar{q}$ pair created is virtual. These quarks then interact via a T matrix, which describes the interaction of a virtual (off-mass-shell) $q\bar{q}$ pair, and are then annihilated. The study of correlators, constructed with a variety of quark "currents," provides information concerning $q\bar{q}$ resonances and bound states [1]. If we consider the Fourier transform of the scalar-isoscalar correlator, $iC_S(P^2)$, we find, in the absence of coupling to the two-pion continuum,

$$C'_S(P^2) = -\frac{J'_S(P^2)}{1-G_SJ'_S(P^2)} \ , \tag{6.5}$$

rather than

$$C_S(P^2) = -\frac{J_S(P^2)}{1-G_SJ_S(P^2)} \ . \tag{6.6}$$

Coupling to the two-pion continuum may be introduced using the methods of Ref. [10] and the result of the evaluation of the third diagram in Fig. 4(b). (We note again, that if $C_S(P^2)$ is obtained in this fashion, the only singularities are those due to the two pions going on-mass-shell.) We also remark that, in Ref. [10], we saw that $C_S(P^2)$ could be well represented by a σ-dominance model for *spacelike* P^2, even if there was no *physical* low-mass σ in the model. To the extent that $J'_S(P^2)$ is close in value to $J_S(P^2)$, *for spacelike* P^2, our observation [10] concerning the validity of a σ-dominance representation (for $P^2 \leq 0$) would still be appropriate. That observation will still be true, when we consider coupling to the two-π continuum, if the third diagram in Figs. 4(a) and 4(b) have similar values for spacelike P^2.

As a final point, we remark that several authors [6,14] have studied flavor-SU(3) versions of the NJL model, supplemented with instanton effects. Studies of meson spectra have been extended to masses of the order of 1 GeV, even though the model has a continuum starting at $2m_q$. We believe that the vertex function studied in this work will be of use in justifying, in part, such calculations made using the standard NJL model, which does not describe confinement.

ACKNOWLEDGMENTS

This work was supported in part by a grant from the National Science Foundation and the PSC-CUNY Faculty Research Program.

APPENDIX A: ANALYSIS OF AN EQUATION FOR THE VERTEX FUNCTION

In this appendix we wish to understand how the integral equation for the vertex function yields a solution for $\Gamma(P^0,|\mathbf{k}|)$ that has $\Gamma(P^0,k_{\rm on}) = 0$. To understand this feature, we use the model of Sec. II. There $a(k)$ was defined by Eq. (2.12) and $b(\mathbf{k},\mathbf{k}')$ was given by Eqs. (2.13) and (2.14). Using the Green's function of Eq. (2.8) and $K(\Delta^2)$ of Eq. (3.2), we write

$$\Gamma(P^0,|\mathbf{k}|) = 1 + \int d\mathbf{k}'K(\Delta^2)g(P^0,|\mathbf{k}'|) \times \frac{b(\mathbf{k},\mathbf{k}')}{a(\mathbf{k})}\Gamma(P^0,|\mathbf{k}'|) \ . \tag{A1}$$

Now we note that $K(\Delta^2)$ is largest for $\Delta^2 = 0$ and falls off rapidly as Δ^2 is increased from zero. Therefore, the integral over $\mathbf{k}'$ only has important contributions for $\mathbf{k} \simeq \mathbf{k}'$. It is then useful to expand $\Gamma(P^0,|\mathbf{k}'|)$ about the value of $|\mathbf{k}'| = |\mathbf{k}|$:

$$\Gamma(P^0,|\mathbf{k}'|) = \Gamma(P^0,|\mathbf{k}|) + (|\mathbf{k}'| - |\mathbf{k}'|)\cdot\Gamma'(P^0,|\mathbf{k}|) + \cdots \ . \tag{A2}$$

Results that are accurate to about 80% may be obtained if only the first term of Eq. (A2) is kept. Then, in that very simple approximation, we have

$$\Gamma(P^0,|\mathbf{k}|) = 1 + a^0(P^0,|\mathbf{k}|)\Gamma(P^0,|\mathbf{k}|) \ , \tag{A3}$$

with

$$a^0(P^0,|\mathbf{k}|) = \int d\mathbf{k}' g(P^0,|\mathbf{k}'|)\frac{b(\mathbf{k},\mathbf{k}')}{a(\mathbf{k})}K(\Delta^2) \ . \tag{A4}$$

Thus, to a first approximation, we have

$$\Gamma^{(0)}(P^0,|\mathbf{k}|) = \frac{1}{1-a^0(P^0,|\mathbf{k}|)} \ , \tag{A5}$$

where

$$a^0(P^0,|\mathbf{k}|) = -\int_0^\infty d|\mathbf{k}'|\frac{\kappa}{\pi}\left(\frac{m_q}{E(\mathbf{k}')}\right)^2\frac{1}{P^0-2E(\mathbf{k}')} \times\frac{\mathbf{k}'^2}{\mathbf{k}^2}\{aA_{02}+bA_{03}+cA_{12}+dA_{13}\} \ . \tag{A6}$$

See Eqs. (3.3)–(3.9).

We now write

$$a^0(P^0,|\mathbf{k}|) = \int_0^\infty d|\mathbf{k}'|g^0(P^0,|\mathbf{k}'|)f(P^0,|\mathbf{k}|,|\mathbf{k}'|) \ , \tag{A7}$$

where

$$g^0(P^0,|\mathbf{k}'|) = \frac{1}{k_{\rm on}^2-\mathbf{k}'^2} \tag{A8}$$

and

$$f(P^0,|\mathbf{k}|,|\mathbf{k}'|) = -\left(\frac{m}{E(\mathbf{k}')}\right)^2\left(\frac{\mathbf{k}'^2}{\mathbf{k}^2}\right)\frac{P^0+2E(\mathbf{k}')}{4} \times\{aA_{02}+bA_{03}+cA_{12}+dA_{13}\} \tag{A9}$$

with $k_{\rm on}^2 = P_0^2/4 - m_q^2$.

We find that $a^0(P^0,|\mathbf{k}|)$ is large and positive for $|\mathbf{k}|$ somewhat less than $k_{\rm on}$. Further, $a^0(P^0,|\mathbf{k}|)$ is large and negative for $|\mathbf{k}|$ somewhat greater than $k_{\rm on}$. (See Fig. 10.) This behavior leads to values for $\Gamma(P^0,|\mathbf{k}|)$ similar to those shown in Fig. 5 for $P^0 > 2m_q$. [Still more accurate results are obtained, if we keep the second term on the right-hand side of Eq. (A2).]

In order to understand the behavior of $a^0(P^0,|\mathbf{k}|)$ shown in Fig. 10, it is useful to graph $g^0(P^0,|\mathbf{k}'|)$ and $f(P^0,|\mathbf{k}|,|\mathbf{k}'|)$ versus $|\mathbf{k}'|$, for fixed P^0 and $|\mathbf{k}|$. Let us take $P^0 = 0.8$ GeV and $m_q = 0.33$ GeV. Then $k_{\rm on} = 0.23$ GeV. Thus, $g^0(P^0,|\mathbf{k}'|)$ has the form shown in Figs. 11–13 (solid curve). [The vertical line denotes the value of $k_{\rm on}$.] In Fig. 11, we have $|\mathbf{k}| = 0.8$ GeV, in Fig. 12 we have $|\mathbf{k}| = 0.3$ GeV, and in Fig. 13 we have $|\mathbf{k}| = 0.1$ GeV. In these figures, the dotted curve is $f(P^0,|\mathbf{k}|,|\mathbf{k}'|)$. As expected, $f(P^0,|\mathbf{k}|,|\mathbf{k}'|)$ is large for $|\mathbf{k}'| = |\mathbf{k}'|$. (The peaks have a width at half-maximum of about μ, which is here equal to 0.050 GeV.) With the use of smaller values of μ, the peaks would appear more like delta functions, so that $|\mathbf{k}|'$ would need to be very close to $|\mathbf{k}|$ to get a sizable value for f.

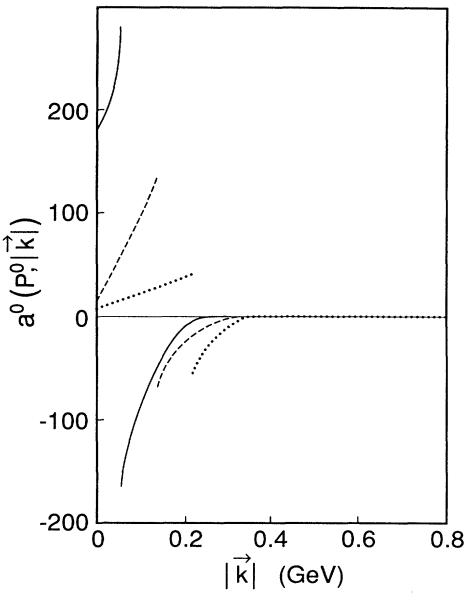

FIG. 10. Values of $a^0(P^0,|\mathbf{k}|)$ are shown for $P^0 = 0.67$ GeV (solid line), $P^0 = 0.72$ GeV (dashed line), and $P^0 = 0.80$ GeV (dotted line). Note that $a^0(P^0,|\mathbf{k}|)$ goes to plus (minus) infinity as $|\mathbf{k}|$ approaches $k_{\rm on}$ from below (above). (Here $m_q = 0.33$ GeV, $\mu = 0.050$ GeV, and $\kappa = 0.3$ GeV^2.)

From inspection of Figs. 10–13 one can see how the behavior of the potential for $\mathbf{k}' \sim \mathbf{k}$ governs the behavior of $a^0(P^0,|\mathbf{k}|)$, which, in turn, determines the behavior of $\Gamma(P^0,|\mathbf{k}|)$. In this manner, we can trace the result that $\Gamma(P^0,k_{\rm on})$=0 to the infrared behavior of the (confining) interaction.

We can demonstrate, in a more direct fashion, that $\Gamma(P^0,k_{\rm on}) = 0$ if the interaction is confining. Let us consider a nonrelativistic version of our problem, such that V is the confining potential and

$$\Gamma_{\rm NR}(s,k) = 1 + \int dk''dk'\Gamma_{\rm NR}(s,k'') \times\langle k''|G_0(s)|k'\rangle\langle k'|V|k\rangle \ . \tag{A10}$$

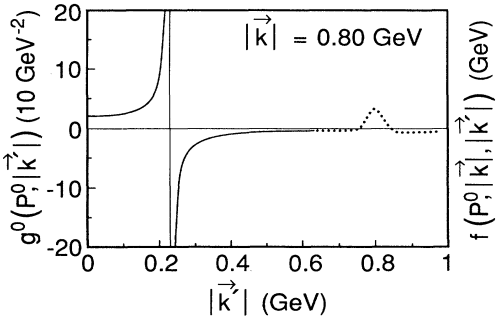

FIG. 11. Values of $g^0(P^0,|\mathbf{k}|)$ are shown as a solid line and values of $f(P^0,|\mathbf{k}|,|\mathbf{k}'|)$ are given by the dotted line. Here $|\mathbf{k}| = 0.80$ GeV, $P^0 = 0.80$ GeV, $\mu = 0.050$ GeV, and $\kappa = 0.30$ GeV^2.

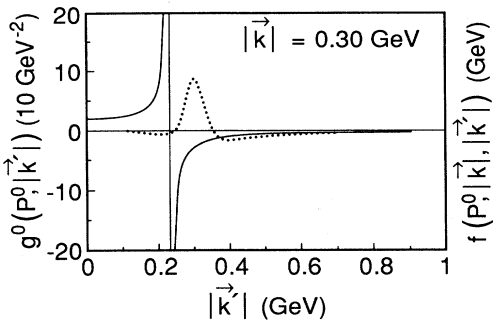

FIG. 12. Same caption as Fig. 11, except that $|\mathbf{k}| = 0.30$ GeV.

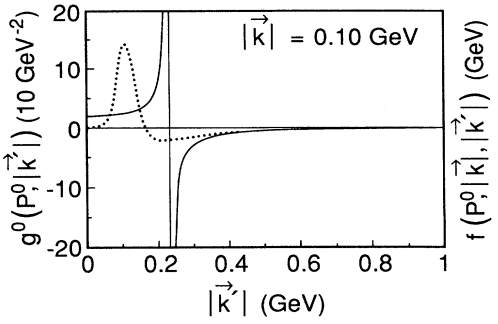

FIG. 13. Same caption as Fig. 11, except that $|\mathbf{k}| = 0.10$ GeV.

Here, the on-shell condition is $k = k_{\rm on} = \sqrt{s}$. Further,

$$\langle k''|G_0(s)|k'\rangle = \frac{\delta(k''-k')}{s-k'^2+i\epsilon} \tag{A11}$$

is the free Green's function. It is useful to rewrite Eq. (A10) in terms of a complete Green's function, $G(s)$, such that Eq. (A10) becomes

$$\Gamma_{\rm NR}(s,k) = 1 + \int dk''dk' \langle k''|G(s)|k'\rangle\langle k'|V|k\rangle \ . \tag{A12}$$

Now, consider the limit of $\mu \to 0$, so that our problem has only bound-state solutions generated by the linearly rising potential. Then

$$\langle k''|G(s)|k'\rangle = \sum_B \frac{\langle k''|\psi_B\rangle\langle\psi_B|k'\rangle}{s-\kappa_B^2} \ , \tag{A13}$$

where the $\langle k|\psi_B\rangle$ are bound-state wave functions. Using Eqs. (A12) and (A13), we have

$$\Gamma_{\rm NR}(s,k) = 1 + \sum_B \int dk''dk' \times \frac{\langle k''|\psi_B\rangle\langle\psi_B|k'\rangle\langle k'|V|k\rangle}{s-\kappa_B^2} \ . \tag{A14}$$

Here, we see that $\Gamma_{\rm NR}(s,k)$ has poles at $s = \kappa_B^2$. Now, use the equation satisfied by $\langle k|\psi_B\rangle$,

$$(\kappa_B^2 - k^2)\langle k|\psi_B\rangle = \int dk' \langle k|V|k'\rangle\langle k'|\psi_B\rangle \ , \tag{A15}$$

to rewrite Eq. (A14) as

$$\Gamma_{\rm NR}(s,k) = 1 + \sum_B \int dk'' \langle k''|\psi_B\rangle\langle\psi_B|k\rangle \frac{(\kappa_B^2-k^2)}{s-\kappa_B^2} \ . \tag{A16}$$

Now, when $k^2 = k_{\rm on}^2 = s$, we find

$$\Gamma_{\rm NR}(s,k_{\rm on}) = 1 - \sum_B \int dk'' \langle k''|\psi_B\rangle\langle\psi_B|k\rangle \tag{A17}$$

$$= 1 - \int dk'' \delta(k-k'') \tag{A18}$$

$$= 0 \ . \tag{A19}$$

The corresponding relation in the relativistic problem is $\Gamma(P^0, k_{\rm on}) = 0$. For the potential, $V(r) = \kappa r e^{-\mu r}$, used in this work we do not encounter any bound-state poles of $\Gamma(P^0, |\mathbf{k}|)$ in the region of interest, $P^0 < 1$ GeV. That feature accounts for the rather smooth behavior of $\Gamma(P^0, |\mathbf{k}|)$ as P^0 is varied that is seen in Figs. 5, 7, and 8.

[1] For a recent review of hadronic current correlation functions, see E. Shuryak, Rev. Mod. Phys. **65**, 1 (1993).

[2] L.S. Celenza, C. M. Shakin, Wei-Dong Sun, J. Szweda, and Xiquan Zhu, Ann. Phys. (N.Y.) (to be published).

[3] L. S. Celenza, C. M. Shakin, Wei-Dong Sun, and J. Szweda, Brooklyn College Report No. BCCNT 93/091/234, 1993 (unpublished).

[4] Y. Nambu and G. Jona-Lasinio, Phys. Rev. **122**, 345 (1961); **124**, 246 (1961). Note that this model dealt with nucleon degrees of freedom, since it predates the quark model.

[5] L. S. Celenza, C. M. Shakin, and J. Szweda, Int. J. Mod. Phys. E **2**, 437 (1993).

[6] V. Vogl and W. Weise, Prog. Part. Nucl. Phys. **27**, 195 (1991).

[7] F. Gross and J. Milana, Phys. Rev. D **43**, 2401 (1991).

[8] F. Gross and J. Milana, Phys. Rev. D **45**, 969 (1992).

[9] We have found the momentum-space bosonization described in V. Bernard, A. A. Osipov, and Ulf-G. Meissner, Phys. Lett. B **285**, 119 (1992) to be quite useful when we perform calculations in momentum space.

[10] L. S. Celenza, C. M. Shakin, Wei-Dong Sun, J. Szweda, and Xiquan Zhu, Int. J. Mod. Phys. E **2**, 603 (1993).

[11] Nan-Wei Cao, C. M. Shakin, and Wei-Dong Sun, Phys.

Rev. C **46**, 2535 (1992).

[12] Procedures for solving two-body, momentum-space, relativistic equations with confining potentials have recently been considered by K. M. Maung, D. E. Kahana, and J. W. Norbury, Phys. Rev. D **47**, 1182 (1993). For restrictions on the form of the $q\bar{q}$ interaction due to chiral symmetry, see, for example, J. E. Villate, D-S. Liu, J. E. Ribeiro, and P. J. deBicudo, Phys. Rev. D **47**, 1145 (1993).

[13] R. Blankenbecler and R. Sugar, Phys. Rev. **142**, 1051 (1966); V. G. Kadyshevsky, Nucl. Phys. **B6**, 125 (1968); M. Thompson, Phys. Rev. D **1**, 110 (1971); R. M. Woloshyn and A. D. Jackson, Nucl. Phys. **B64**, 269 (1973); F. Gross, Phys. Rev. **186**, 1448 (1969).

[14] M. Takizawa, K. Tsushima, Y. Kohyama, and K. Kubodera, Nucl. Phys. **A507**, 611 (1990); Prog. Theor. Phys. **82**, 481 (1989); S. Klimt, M. Lutz, U. Vogl, and W. Weise, Nucl. Phys. **A516**, 429 (1990); V. Vogl, M. Lutz, S. Klimt, and W. Weise, *ibid.* **A516**, 469 (1990); R. Alkofer and I. Zahed, Phys. Lett. B **207**, 482 (1988).